كلية الهندسة بشبرا
FACULTY OF ENGINEERING AT SHOUBRA
ERJ
PRINT ISSN 3009-6049
ONLINE ISSN 3009-6022

ENGINEERING RESEARCH JOURNAL (ERJ)
Volume (53),Issue (1)
January 2024, pp:279-291
https://erjsh.journals.ekb.eg

Effect of baffle configuration on the thermal performance attributes of shell and semi-circular tube heat exchangers

N.M. Almulla [1], M.A. Moawed [1], M.A. Abd-Elrahman [1], Mohamed R. Salem [1,*]

[1]*Mechanical Engineering Department, Faculty of Engineering at Shoubra, Benha University, 108 Shoubra St., 11629, Cairo, Egypt*
**Corresponding author*

E-mail address: dr.n.almulla77@gmail.com , mmoawed28@feng.bu.edu.eg , mohamed.abdelrahman@feng.bu.edu.eg , mohamed.abdelhamid@feng.bu.edu.eg

Abstract: This study aims to improve the performance characteristics of a shell-tube heat exchanger in counterflow configuration. It considers the effect of using baffles and semicircular tubes as heat transfer surfaces. Twenty-nine heat exchangers are designed and constructed, consisting of tubes of circular or semicircular tubes (SCTs) with base spacing ratios (β) ranging from 23.6% to 55.1%. The examined baffles have a pitch ratio (λ) of 1.47 to 2.36, a total cut ratio (δ) of 16.5% to 25% and have two cutting configurations: edge cutting with a cutting ratio (ψ) of 0% to 16.5% and internal cutting baffles with a cutting ratio (τ) of 0% to 16.5%. The experiments are done for Reynolds ($3550 \leq Re_{sh} \leq 14580$) and Prandtl numbers ($4.47 \leq Pr_{sh} \leq 7.28$). The results show that using baffles and/or SCTs increases the heat transfer rate and pressure loss, and when the SCT spacing ratio increases and baffles cut and pitch ratios decrease, these performance metrics significantly rise. However, baffles with edge cutting are better than those with internal cutting. The hydrothermal performance index is evaluated using the Stanton number of the shell side and f_{sh} ratios, with a maximum value of 2.54 achieved by utilizing baffles of δ = ψ = 16.5%, τ = 0, λ = 1.47, and SCTs of β = 55.1%, and lowest shell-side flow rate and inlet temperature. Finally, correlations are introduced to predict $\overline{Nu}_{sh}$ and f_{sh}, besides the performance index of the tested heat exchangers .

Keywords: Heat exchanger; Baffles cut ratio; Baffles pitch ratio; Cutting configuration; Semi-circular tube.

1. Introduction

Heat transfer is crucial in energy conversion, usage, and recovery in various sectors. Shell and tube heat exchangers are widely used due to their adaptability, high efficiency, and flexibility. They are highly customizable and can be designed with unique features to meet specific requirements [1,2]. However, precise measurement of heat transfer rate and pressure drop calculations are challenging. Designing suitable heat exchangers relies on understanding heat exchange and flow resistance behaviours. To increase heat transfer rate with less pumping power, various methods exist, including active and passive approaches. Compound enhancement, combining active and passive approaches, increases heat transfer beyond what would be achieved with one method alone [3-6].

One of the displacement augmentation tools could be baffles. They are displacement augmentation tools used in industrial process vessels like heat exchangers, chemical reactors, and static mixers. They support tubes, direct fluid back and forth, remove dead spots, increase heat transfer rate, and minimize temperature differences. These solid or perforated baffles are commonly used in heat exchangers for heating, chilled water, groundwater, and residential applications [5].

Numerous scientific works have been published on the performance behaviour of conducting baffles in various heat exchange processes. [7] studied baffle pitch's impact on heat transfer area and friction loss in heat exchanger shells. They found that the baffle pitch ratio significantly affects pumping power and heat transfer area. They proposed a formula for calculating the optimal baffle pitch for single-phase heat exchangers. [8] studied unstable heat transfer augmentation in laminar flow channels with in-line and staggered baffles. They found the in-line baffle structure had a higher Nusselt number and nearly identical friction factors. [9] studied the impact of baffle-wall distance on local heat transfer in rectangular channels with oscillatory flow. Results showed that short baffle widths reduce heat transfer coefficients, while wide widths result in a greater heat transfer coefficient. [10] studied the impact of a single baffle on heat transmission and friction properties in a rectangular channel. The study found that increasing the flow Reynolds number, baffle inclination angle, and reducing the baffle cut ratio improved the average Nusselt number. However, the equal friction factor criteria performance study showed that the inlet baffle was not thermodynamically favourable for heat transfer enhancement. Yang and Hwang's numerical predictions [11] showed turbulent fluid flow and heat transfer characteristics in a rectangular channel with staggered solid and perforated baffles. Different flow patterns affect local heat transfer coefficient distributions, with porous-type baffle channels having lower friction factors. [12] studied heat transfer and friction loss properties in a rectangular channel with inclined solid and perforated baffles. They found that the second baffle plate's position, orientation, and shape significantly influenced the Nusselt number and friction factor. [13] conducted an energy dissipation

analysis on nine circular tubes with baffle plate inserts. They found that baffled tubes have larger unsteady dissipation energy criteria than smooth tubes, with a range of air Reynolds numbers from 3000 to 20000. [14] improved a shell-and-tube heat exchanger's shell-side layout by installing sealers, closing gaps, reducing short-circuit flow, and improving heat transfer coefficient. Pressure losses increased, but the increase in pump power was ignored compared to the increase in heat flux.

[15] studied turbulent airflow in a rectangular channel with rectangular and trapezoidal baffles. They found trapezoidal baffles gained velocity per contribution, but increased friction coefficient. [16] studied laminar periodic flow and heat transmission in a rectangular channel with triangular wavy baffles. They found that triangular wavy baffles were more effective than without baffles for heat transfer. [17] studied heat transport in a rectangular channel with two corrugated fins. They found that shortening fin distance increased Nusselt number and pressure loss. Increasing Reynolds number increased heat transmission but eliminated fin ripple impact on pressure decrease beyond 15000. [18] found that helical baffles have lower pressure drop and higher heat transfer coefficient, making them beneficial for shell-and-tube oil coolers with segmental and helical baffle designs. [19] studied forced convection heat transfer and pressure drop in a horizontal duct with baffles at different inclination angles. They found that increasing baffle inclination improves heat transmission and increases pressure drop. Hussein's study [20] on turbulent flow and heat transfer in a double pipe counter water flow heat exchanger revealed that baffle pitch and Reynolds number significantly impact thermal performance. The smallest pitch spacing resulted in the highest performance ratio, while the Nusselt number and friction factor were larger in smooth tubes. [21] studied turbulent forced convection, heat transfer, and performance enhancement in a square channel with discrete combination baffles. They found that discrete mixed baffles increased heat transfer rate and thermal efficiency. [22] improved heat transfer efficiency and pressure drop by replacing segmental baffles with inclined type, revealing increased performance and reduced pressure drop. [23] studied turbulent flow and heat transfer in a dimple square duct with inline angled baffles. The experiment found higher heat transfer rates and friction factors, with the maximum heat transfer occurring at pitch ratio = 0.83 and a maximum thermal performance enhancement factor of 2.4 at Re = 3900.

In their experimental and numerical studies, Salem et al. [5] and [24], they found that perforated baffles increased Nusselt number and friction factor in horizontal double pipe heat exchangers while decreasing pitch ratio decreased them. Correlations were found between baffles and concentric tube heat exchangers. Besides, [25] studied the hydrothermal performance of horizontal double pipe heat exchangers with and without helical tape inserts, finding increased Nusselt number and friction factor. [28] found that baffles significantly affect pressure drop in shell and tube heat exchangers, with double segmental baffles reducing vibrational damage and helical baffles improving heat transfer and pumping power. [27] studied heat transfer and pressure drop in a shell and tube heat exchanger with six porous baffles. They found low baffle cuts improved heat transmission, but increased pressure drops. An artificial neural network was trained to determine optimal parameters, maximizing heat transmission while minimizing pressure drop. [28] studied shell-and-tube heat exchanger performance using ANSYS Fluent, finding small dead zones for 40° baffle inclination, but increased baffle angle decreased performance factors. [29] simulated a shell and tube heat exchanger with segmental baffles, finding optimal baffle cuts and spacings for efficient functioning. Results showed increased heat transfer coefficient and acclivity, while pressure drop increased with increasing spacing. [30] utilized a reinforcement learner algorithm to optimize thermal performance, Nusselt number, and friction factor in double-pipe heat exchangers with perforated baffles. Boonloi and Jedsadaratanachai's CFD analysis [31] found the best heat transfer rate in a baffled duct, with an optimum thermal enhancement factor of 4.06. [32] studied the hydraulic and thermal performance of inclined baffled channels under pulsing flow conditions, finding thermal enhancement enhanced by pulsation frequency, amplitude, Reynolds number, and heat transmission increase.

This review of the literature indicates that there have been numerous studies on the results of adding baffles of different shapes to different duct configurations. Most of these studies looked at how baffle geometry affected fluid flow in rectangular channels. They also showed that the characteristics of heat transmission and pressure drop were significantly influenced by the configuration, arrangement, cut ratio, and pitch between the baffles. As well, these studies also looked at how installing baffles affected the efficiency of heat exchange when using circular tubes as the heat transfer surface. Recent research [33-36] suggested that SCTs, with their larger heat transfer surface areas, offer faster heat transfer rates than CCTs. Therefore, the present work is devoted to experimentally investigating the hydrothermal attributes of a shell-tube heat exchanger of a counter-flow configuration including the combined passive techniques of SCTs and single segmental baffles. The experiments examine the impact of baffle cut and pitch ratios in addition to the impact of baffle edge and/or internal cut configurations. These are for a wide range of shell-side operating conditions and for various SCT base spacing ratios. Correlations to predict the average Nusselt number ($\overline{\mathrm{Nu}}_{\mathrm{sh}}$) and Fanning friction factor (f_{sh}) for the shell-side of the heat exchanger with both baffles and SCTs, as well as the hydrothermal performance index (HTPI) to assess the performance of the heat exchanger with incorporating the proposed technique when compared to the corresponding performance of the conventional heat exchanger, are planned.

2. Experimental apparatus

The setup in this study comprises hot and cold loops: the hot circuit includes a heating cabinet, pump, valves, a flow

meter, and connecting pipes. Besides, a cooling system, pump, valves, a shell, a flow meter, and connecting pipes make up the cold circuit as presented in Figs. 1 & 2. To heat the water to the required temperature, four horizontally mounted 5 kW electric heaters were installed in the heating cabinet, while two cooling units (20.5 kW) were engaged with the cooling cabinet to remove the heat energy from the other circuit. Four ports were prepared on each cabinet, two on the top cover for the bypass line and heat exchanger and two on the bottom for the drain exit points. Moreover, two 3-hp centrifugal pumps with maximum flow rates of 110 l/min were utilized: Pump-1 moved the heating water from the tank, flow meter-1 measured it, and then the water was pumped back into the heating tank. While Pump-2 moved cooling water, which then recirculated through the heat exchanger's outer shell before being pumped back into the cooling tank. Furthermore, PVC and flexible nylon tubing using T-shaped connectors were engaged to connect the differential pressure transducer and shell main line.

With various geometrical parameters for the tubes and baffles, 29 shell and tube heat exchangers with a counter-flow configuration are built. The heat exchangers that were tested have either 14 SCTs or 7 CCTs. The copper tubes have an overall length of 1250 mm for each tube and have outer and inner diameters of 12.7 and 11.5 mm, respectively. The tubes were arranged with spacings from centre to centre of 25 mm. An SCT is formed by longitudinally cutting off a CCT with a plasma cutting tool. The next step involves longitudinally soldering a sheet that is the same material, length, diameter, and thickness. Any protuberances that the welding process may have produced on either side of the SCT are carefully removed. Mild steel (2 mm wall thickness) is used to construct the heat exchangers' outer shell, which is rolled into a cylindrical shape (101.6 mm inner diameter and 1200 mm length) before welding. On both ends of the heat exchanger's shell, which will be bolted to the headers, two flanges (6 mm wall thickness) are welded.

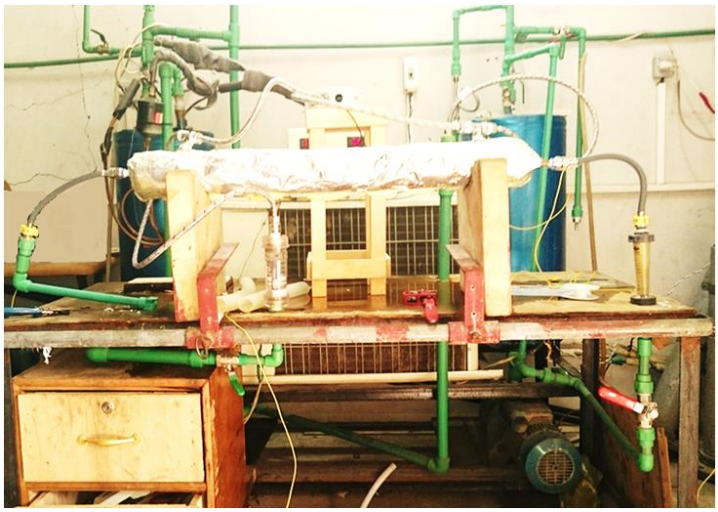

Fig. 1 Photo of the current experimental apparatus.

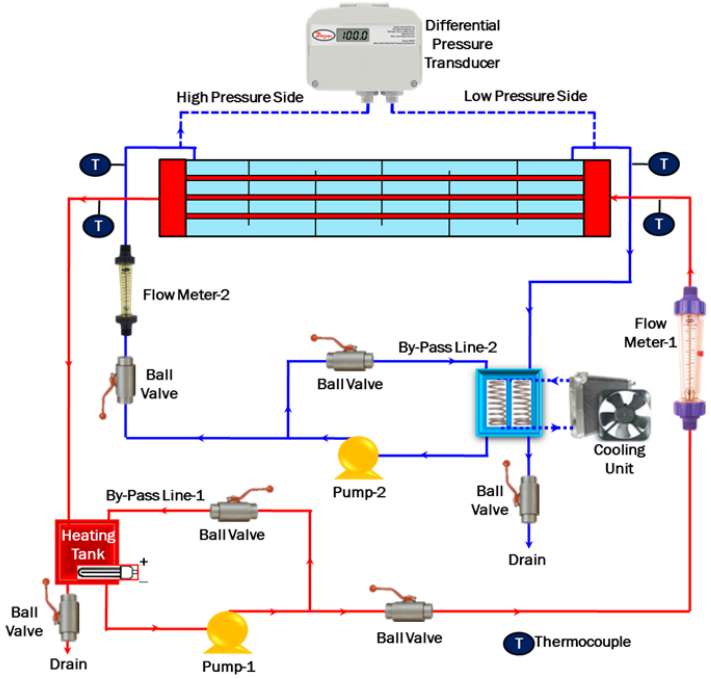

Fig. 2 Schematic layout of the current setup.

The current apparatus includes two cylindrical galvanized steel tanks with a 2 mm wall thickness and an inner diameter and length of 101.6 mm and 120 mm, respectively. These tanks are used to receive water going into and coming out of the tubes. Each header has two nipples, each with a 4 mm wall thickness and made of the same material. To seal off these ends, one end of each header is bolted to a blind flange. The other ends are fastened to the shell's flanges by bolts. In total, 58 circular housing dies with holes that are the same size and number as the tubes of the heat exchanger being tested are used. These dies are made of galvanized steel and have a 3 mm wall thickness. They are placed between the header and shell nipples. Using a laser-cut machine, they are drilled. A schematic representation of the header and the housing die is revealed in Fig. 3.

To prevent leaks, each header contains three rubber gaskets: one is positioned between the header nipple and the blind flange, while the other two are positioned at the opposite end between the housing die and the shell nipple. The two headers and the CCTs/SCTs are further connected by way of the dies. The potential gap between the tubes and the die's holes is carefully sealed off. A copper sheet with a thickness of 0.6 mm is used to make the baffles, which are then cut and drilled using a laser. The heat exchanger shell's 101.6 mm diameter is the same for all baffles, giving them all a circular shape. Then the baffles are soldered to the tubes using copper welding to keep their positions. Table 1 lists the distinctive characteristics of the various configurations of the incorporated heat exchangers, and Fig. 4 illustrates an SCT with its primary geometrical characteristics, while schematic diagrams of the baffles are displayed in Fig. 5. Additionally, the shell has welded-on inlet and exit ports with constant cross sections, 30mm centres, and thermally isolated outer surface with ceramic fibre, asbestos rope, and glass wool.

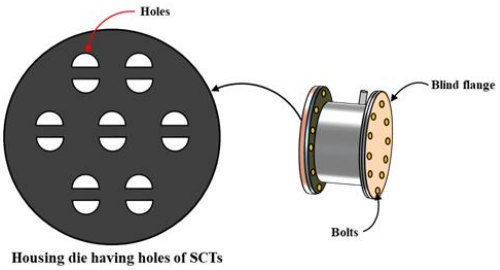

Fig. 3 The header of the heating water.

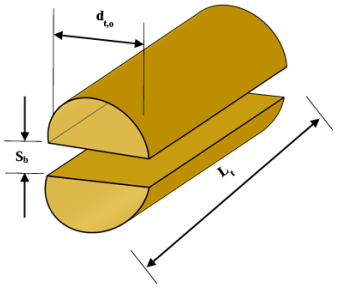

Fig. 4 The fundamental shape of an SCT.

Table 1 Key parameters of examined heat exchangers.

#Runs	S_b (mm)	β	δ	ψ	τ	p_{baffle} (mm)	N_{baffle}	λ
18	CCT		No baffles					
36			16.5%	16.5%	0	200	6	1.97
54			20.0%	20.0%				
72			25.0%	25.0%				
90			16.5%	16.5%		240	5	2.36
108						150	8	1.47
126	3	23.6%	No baffles					
144	5	39.4%						
162	7	55.1%						
180	3	23.6%	16.5%	16.5%	0	200	6	1.47
198			20.0%	20.0%				
216			25.0%	25.0%				
234			16.5%	9.4%	7.1%			
252			20.0%	12.9%				
270			25.0%	17.9%				
288	5	39.4%	16.5%	16.5%	0			
306			20.0%	20%				
324			25.0%	25%				
342			16.5%	4.7%	11.8%			
360			20.0%	8.2%				
378			25.0%	13.2%				
396	7	55.1%	16.5%	16.5%	0			
414			20.0%	20%				
432			25.0%	25%				
450			16.5%	0	16.5%			
468			20.0%	3.5%				

486			25.0%	8.5%				
504			16.5%	16.5%	0	240	5	2.36
522						150	8	1.47

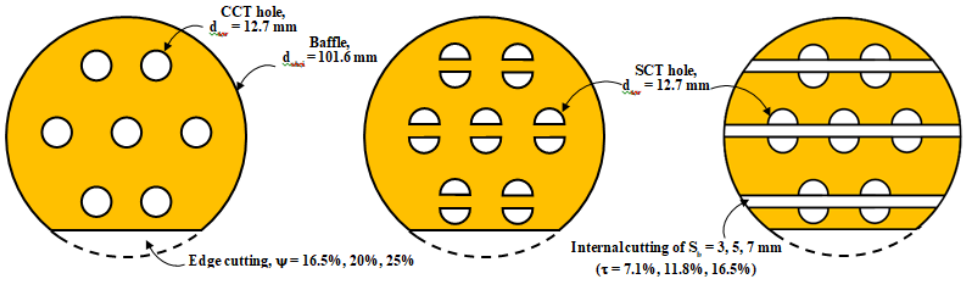

(a) Baffle of edge cutting for CCTs (b) Baffle of edge cutting for SCTs (c) Baffle of edge and internal cutting for SCTs

Fig. 5 Key attributes of the incorporated baffles in the current study.

$$\beta = \frac{S_b}{d_{t,o}} \quad (1)$$

$$\psi = \frac{A_{Edge\ cut}}{A_{Baffle}} \quad (2)$$

$$\tau = \frac{\sum A_{Internal\ cut}}{A_{Baffle}} \quad (3)$$

$$\delta = \gamma + \tau \quad (4)$$

$$\lambda = \frac{p_{Baffle}}{d_{Baffle}} \quad (5)$$

The volume flow rates of the fluids in the main loop are measured by two calibrated flow meters. Hot fluid loop flow is measured by flow meter-1 at 10 to 100 l/min, while cold fluid line flow is measured by flow meter-2 at 1.8 to 18 l/min. The manufacturer's data sheet states that their reading accuracy is 5%. In addition, four calibrated K-type thermocouples that are inserted 50mm from the heat exchanger ports measure the inlet and exit temperatures of shell and tube fluids. The thermocouples are connected by a selector switch and the temperature is displayed on a digital thermometer with a resolution of 0.1°C. Additionally, a calibrated digital differential pressure transducer with a working range of 0–103.4 kPa measures the pressure of liquid and gas in a heat exchanger shell with a 1% accuracy.

3. Experimental procedures

The thermocouples are first attached to the inlet and outlet of the shell and tube sides. The shell-tube heat exchanger, heating and cooling units, pumps, piping, flow meters, thermocouples, and differential pressure gauge are then assembled to start the experiments. The first step in gathering data from the system was to fill the heating and cooling tanks with water from the domestic water supply. Then, the heater, cooler, and pumps were turned on. On the 29 heat exchangers depicted in Table 1, a series of 522 experiments were conducted. Test operation is in steady-state condition when thermocouple readings show a maximum 0.5°C variation within 20 minutes, and fluid inlet and outlet temperatures remain stable, less than 0.1°C before recording. The range of the operational conditions is provided in Table 2.

Table 2 Range of fluids operating conditions.

Parameters	Range or value
Shell-side flow rate, l/min	8.1-18.4 ($3550 \leq Re_{sh} \leq 14580$)
Shell-side inlet temperature, ℃	15, 20, 25 ($4.47 \leq Pr_{sh} \leq 7.28$)
Tube-side flow rate, l/min	42.7
Tube-side inlet temperature, ℃	60

4. Calculation methodology

The key measurements in heat transfer estimations comprise six variables, the flow rates and inlet/outlet temperatures of both streams of the heat exchanger. The heat transfer rates on the tube and shell sides (Q_t and Q_{sh}) are assessed by:

$$Q_t = \dot{m}_t Cp_t\left(T_{t,i} - T_{t,o}\right) \quad (6)$$

$$Q_{sh} = \dot{m}_{sh} Cp_{sh}\left(T_{sh,o} - T_{sh,i}\right) \quad (7)$$

Presuming that the measurements are satisfactorily accurate without heat gain/loss, an energy balance should be between both rates ($Q_t = Q_{sh}$). While in the actual tests, there are some disagreements between them. Therefore, the mean value, Q_{ave}, is applied. For all runs, the heating and cooling loads estimated from the hot and cold sides did not diverge by more than $\pm 4.5\%$.

$$Q_{ave} = \frac{|Q_t| + |Q_{sh}|}{2} \quad (8)$$

$$\Delta Q_{ave}(\%) = \frac{|Q_t| - |Q_{sh}|}{Q_{ave}} * 100 \quad (9)$$

The overall thermal conductance is determined from this heat load, the temperature data, and the heat transfer area applying Eq. (10):

$$U_i A_{t,i} = \frac{Q_{ave}}{\Delta T_{L.M}} \quad (10)$$

$$\Delta T_{L.M} = \frac{(\Delta T_i - \Delta T_o)}{\ln\left[\frac{\Delta T_i}{\Delta T_o}\right]} = \frac{\left(T_{t,i} - T_{sh,o}\right) - \left(T_{t,o} - T_{sh,i}\right)}{\ln\left[\frac{T_{t,i} - T_{sh,o}}{T_{t,o} - T_{sh,i}}\right]} \quad (11)$$

$$A_{t,i} = 7\pi d_{t,i} L_t \quad \text{For CCTs} \quad (12)$$

$$A_{t,i} = 14 d_{t,i} L_t (0.5\pi + 1) \quad \text{For SCTs} \quad (13)$$

The water flow in the internal tubes is turbulent and fully developed where the ratio between the tube length (1.2 m) to its hydraulic diameter ($d_{t,h}$ = 0.0115 m for CCT and 0.00703 m for SCT) is 104.4 and 170.8, respectively. The average Nusselt number of the tube-side ($\overline{Nu}_t$) is estimated by applying Dittus-Boelter [37] correlation, Eq. (14), which is valid for $L_t/d_{t,h} \geq 60$, $0.7 \leq Pr \leq 100$, and $Re \geq 10000$. Now, the heat transfer coefficient on the tube side can be estimated via Eq. (15).

$$\overline{Nu}_t = 0.023 * Re_t^{0.8} * Pr_t^{0.4} \quad (14)$$

$$\overline{h}_t = \frac{\overline{Nu}_t . k_t}{d_{t,h}} \quad (15)$$

$$d_{t,h} = d_{t,i} \quad (16)$$

$$d_{t,h} = \frac{\pi d_{t,i}}{\pi + 2} \quad (17)$$

$$\frac{1}{U_i A_{t,i}} = \frac{1}{\overline{h}_{sh} A_{t,o}} + \frac{1}{\overline{h}_t A_{t,i}} \quad (18)$$

$$\overline{Nu}_{sh} = \frac{\overline{h}_{sh}\, d_{sh,h}}{k_{sh}} \quad (19)$$

$$d_{sh,h} = \frac{d_{sh,i}^2 - 7 d_{t,o}^2}{d_{sh,i} + 7 d_{t,o}} \quad (20)$$

$$d_{sh,h} = \frac{\pi\, d_{sh,i}^2 - 7\pi\, d_{t,o}^2}{\pi\, d_{sh,i} + 7 d_{t,o} (\pi + 2)} \quad (21)$$

$$Re_t = \frac{4\dot{m}_{t,tube}}{\pi d_{t,h} \mu_t} \quad (22)$$

$$Re_{sh} = \frac{4\dot{m}_{sh}}{\pi d_{sh,h} \mu_{sh}} \quad (23)$$

$$St_{sh} = \frac{\overline{Nu}_{sh}}{Re_{sh} . Pr_{sh}} \quad (24)$$

$$f_{sh} = \frac{\Delta P_{sh}\, d_{sh,h}}{2 L_{sh}\, \rho_{sh} u_{sh}^2} = \frac{\Delta P_{sh}\, \pi^2\, \rho_{sh}\, d_{sh,h}^5}{32\, L_{sh}\, \dot{m}_{sh}^2} \quad (25)$$

5. Uncertainty analysis

The method introduced by Kline and McClintock [38] is used to assess the level of uncertainty for each parameter. Table 3 summarizes the uncertainties of key parameters.

Table 3 Max. uncertainties in the primary parameters.

Parameter	Uncertainty (%)
Tube-side Reynolds number	±1.70
Sell-side Reynolds number	±2.00
Tube-side average Nusselt number	±1.40
Tube-side average heat transfer coefficient	±1.41
Sell-side average Nusselt number	±2.70
Shell-side average heat transfer coefficient	±2.95
Overall heat transfer coefficient	±2.24
Shell-side Fanning friction factor	±6.50
Shell-side Stanton number	±3.65
Hydrothermal performance index	±6.10

6. Apparatus validation and data verification

The flow and temperature measurements on the shell side are tracked, and the $\overline{Nu}_{sh}$ and f_{sh} are compared to established correlations, in order to validate the heat transfer coefficients and friction factors. $\overline{Nu}_{sh}$ is compared to Gnielinski [39], Eq. (26), and $\overline{Nu}_{sh}$ for turbulent flow in the water through the shell. Using Filonenko's correlation [40], Eq. (27), and f_{sh} results, the Fanning friction factor is assessed. For shell and CCTs, validation experiments were carried out, and the necessary working conditions are listed in Table 4. With maximum variances of 7.8% and 5.5%, respectively, comparisons showed consistent results for $\overline{Nu}_{sh}$ and f_{sh} determinations, ensuring accuracy in experimental equipment and measurement methods.

$$\overline{Nu}_{sh} = \frac{\frac{f_{sh}}{2}(Re_{sh} - 1000) Pr_{sh}}{1 + 12.7 \sqrt{\frac{f_{sh}}{2}} \left(Pr_{sh}^{2/3} - 1\right)} \left[1 + \left(\frac{d_{sh,h}}{L_{sh}}\right)^{2/3}\right] \quad (26)$$

$$f_{sh} = 0.25 (1.82\, log\, Re_{sh} - 1.64)^{-2} \quad (27)$$

Table 4 Validation operational conditions.

Parameter	Range or Value
Tube-side water flow rate, l/min	42.7 ($Re_t \approx 23070$)
Tube-side inlet temperature, ℃	60 ($Pr_t \approx 3.05$)
Shell-side water flow rate, l/min	8.1-18.4 ($3550 \leq Re_{sh} \leq 9760$)
Shell-side inlet temperature, ℃	15, 20, 25 ($5.52 \leq Pr_{sh} \leq 7.28$)

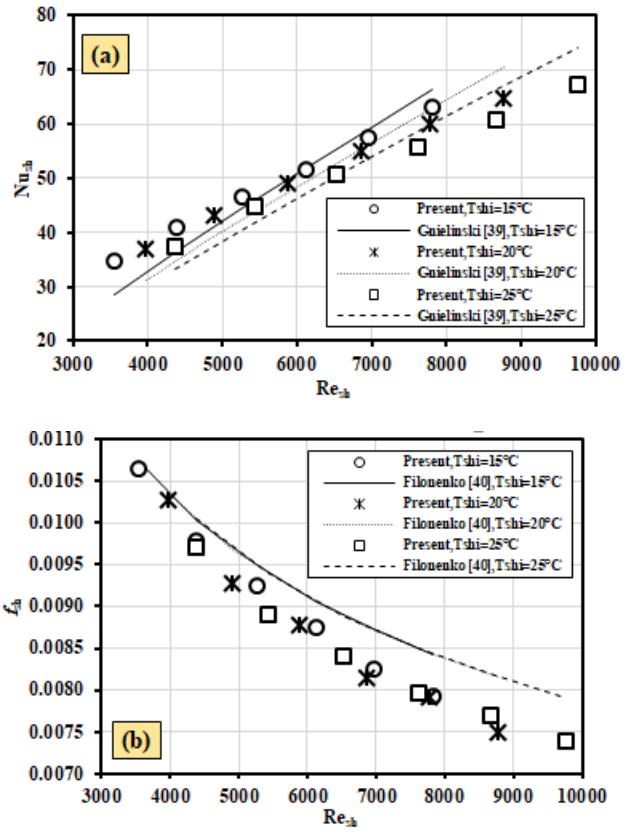

Fig. 6 Outputs of the validation processes: (a) ¯Nu_sh, (b) f_sh.

7. Results and discussions

7.1 Plain heat exchanger with CCT or SCTs at different base-spacing ratios

In this analysis, four heat exchangers; one with CCTs and the other three with SCTs, are subjected to seventy-two experimental testing. The SCTs have bases that are 3 or 5 or 7 mm apart. Thus, the base spacing ratios (β) are 23.6%, 39.3%, and 55.1%, respectively. The operating conditions for the cooling water are adjusted in accordance with Table 2, while the operating conditions for the heating water in the tube side are maintained constant at 60°C input temperature and a total flow rate of 42.7 l/min. Fig. 7 shows the documented results for $\overline{Nu}_{sh}$ in addition to f_{sh} as a consequence of altering the shell side operating circumstances at β = 55.1% as a sample of the findings. It is clear from all runs that $\overline{Nu}_{sh}$ is reduced at the same Re_{sh} as the inlet temperature of the shell-fluid flow rises. This is explained by the fact that when water temperature rises, the Prandtl number falls. In addition, it is clear that $T_{sh,i}$ has a negligibly little impact on f_{sh}. This can be attributed to the lower effect of viscosity variation compared with the inertia force. Furthermore, Fig. 7 makes it clear that raising Re_{sh} augments $\overline{Nu}_{sh}$. This is supported by raising the Reynolds number, which raises the level of fluctuations and causes fluid layers to mix around internal tubes. On the other hand, as Re_{sh} increases, f_{sh} decreases, supporting the idea that momentum forces overcome viscous forces. Additionally, Fig. 8 displays the comparable findings by dividing the internal tubes at various base spacing ratios at $T_{sh,i}$ = 20°C as a sample of the outputs. It is obvious that $\overline{Nu}_{sh}$ and f_{sh} are higher when SCTs are incorporated than when CCTs are. There are various causes for this, one of which is expanding the SCTs' contact area rather than the CCTs' (from $(\pi d_{t,o}L_t)$ for CCT to be $(\pi d_{t,o}L_t + 2d_{t,o}L_t)$ for pair of SCTs). Moreover, as shown in Eqs. (20, 21), dividing the internal tubes results in a smaller shell-side hydraulic diameter, which increases the Reynolds number for the same shell-side flow rate and changes the flow behaviour. Besides, the $\overline{Nu}_{sh}$ and f_{sh} increase with the growth in the SCT spacing ratio. This can be attributed to increasing the flow turbulence level around the tubes by increasing the SCT spacing ratio. This breaks the thermal and velocity boundary layers of the shell-side flow, which increases the flow mixing and consequently increases both the heat transfer rate and shell-side flow resistance. At the smallest spacing ratio between the SCTs (β = 23.6%), the flow velocity beside their bases is very small where the SCTs block the flow at this region, while this is accompanied by a larger spacing between the tube's outer surfaces, which reduces the overall pressure drop. Moreover, the $\overline{Nu}_{sh}$ and f_{sh} rise when the SCT spacing ratio rises. This is explained by the fact that as the SCT spacing ratio is increased, the flow turbulence level around the tubes increases. This causes the thermal and velocity boundary layers of the shell-side flow to be broken. As a result, the heat transfer rate and shell-side flow pressure drop are increased. The flow rate adjacent to the SCTs' bases is very low where they obstruct the flow at this location at the shortest spacing ratio between the SCTs (β = 23.6%) however this is followed by a wider spacing between the tube's outer surfaces, which lowers the overall pressure drop. On the other hand, expanding the SCTs' spacing enables a greater flow of the cooling water on the shell's side between their bases. Moreover, the spaces between the exterior surfaces of the tubes are kept to a minimum. As a result, the flow mixing and turbulence levels around the tube surfaces rise, increasing the heat transfer rate as well as the flow pressure loss on the shell side. Compared with employing CCTS, the average increases in the $\overline{Nu}_{sh}$ are 48%, 63.3%, 80.5% at β = 23.6%, 39.4%, and 55.1%, respectively. The associated increases in the f_{sh} are 1.7%, 9.3%, and 19.5%, respectively.

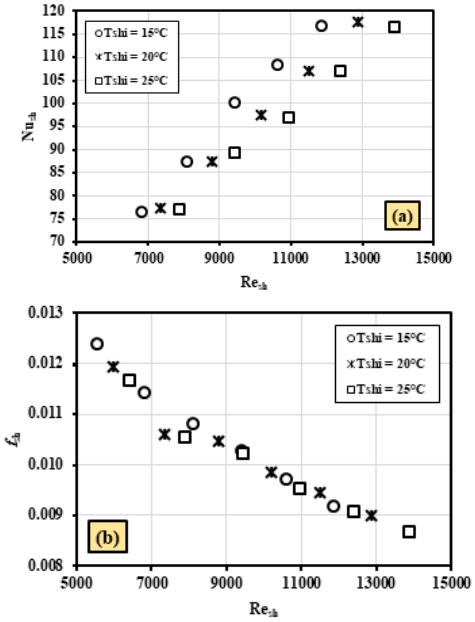

Fig. 7 Performance attributes of investigated heat exchangers vs. Re_{sh} at different shell-side operating conditions (β = 55.1%); (a) $\overline{Nu}_{sh}$, (b) f_{sh}.

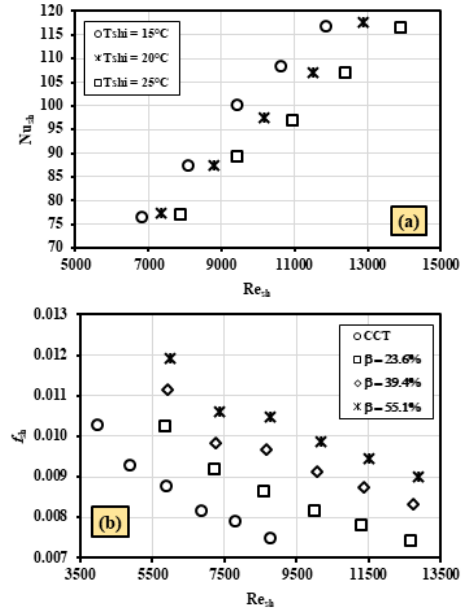

Fig. 8 Performance attributes of investigated heat exchangers vs. Re_{sh} at different base spacing ratios (Tsh, i = 20°C); (a) $\overline{Nu}_{sh}$, (b) f_{sh}.

7.2 Heat exchanger with baffles at several cut ratios/configurations

In this investigation, 378 experimental tests are conducted on 21 heat exchangers, three of which have CCTs and the remaining eighteen have SCTs. The SCTs' bases are spaced 3, 5, or 7 mm apart. The corresponding base spacing ratios are 23.6%, 39.3%, and 55.1%. Each heat exchanger has six single segmental baffles put into its shell with a 200 mm pitch between them (λ = 1.97). Each baffle has a total cut ratio (δ) that ranges from 16.5% to 25%. These cuttings are either done at the edge of the baffle exclusively (using CCTs or SCTs as the heat exchangers) or both the edge and inside of the baffle (conducted with heat exchangers of SCTs only). As shown in Table 1, for the later baffle configuration instance, the edge cut ratio (ψ) is varied between 0 and 25% while the internal cut ratio (τ) is modified between 0 and 16.5%. In these tests, hot water with an inlet temperature of 60°C and a total flow rate of 42.7 l/min is circulated through the tubes while cooling water is passed through the shell of each heat exchanger in accordance with the specifications shown in Table 2. As a sample of the finding, the recorded results for $\overline{Nu}_{sh}$ and f_{sh} are shown for β = 39.3%, λ = 1.97 and $T_{sh,\,i}$ = 20°C in Fig. 9 as a result of introducing baffles of only edge cutting (δ = ψ and τ = 0), while Fig. 10 documents the corresponding outputs with incorporating both edge and internal cuttings in the baffles (δ = ψ + τ and τ = 11.8%, λ = 1.97).

Fig. 9 shows that the baffles' mere existence in the heat exchanger raises $\overline{Nu}_{sh}$ in addition to f_{sh}. When the baffle edge cut ratio is reduced, these performance metrics considerably rise. The average percentage increases in the $\overline{Nu}_{sh}$ are 66.2%, 41.4% and 15.8% at δ = ψ = 16.5%, 20%, and 25%, respectively, in comparison to the situation of no baffles. Besides, 23.2%, 14.5%, and 4.0%, respectively, are the proportional rises in the f_{sh}. They are caused by a decrease in the edge cut ratio (ψ), which increases the throttling of the shell flow and results in better impingement, which significantly increases the pressure drop while also significantly improving heat transfer. In addition, Fig. 10 indicates that the baffles with both edge and internal cuttings still achieve higher shell-Nusselt number and friction factor when compared with no baffle case. The results assure also that the smaller the total cut ratio of the baffles, the greater the shell Nusselt number and friction factor. To judge the associated thermal performance of the heat exchanger due to cutting the baffles internally, the shell side average Nusselt number and friction factor are compared at the same total cut ratio with that resulted by inserting baffles of only edge cutting. The average percentage variations in the $\overline{Nu}_{sh}$ are 11.5%, -3.6% and -6.4% at δ = 16.5%, 20%, and 25%, respectively. Besides, 13.3%, 5.8%, and 13.7%, respectively, are the proportional variations in the f_{sh}.

According to these statistics, baffles with edge cutting are a better tool than those with internal cutting. It is demonstrated that the average Nusselt number of cooling water is larger than that obtained by integrating internal-cutting baffles at the same shell-side Reynolds number. Additionally, the associated shell-side friction factor is lower when edge-cutting baffles are used compared to internal cutting. This is supported by the observation that the internal baffle cutting stifles the fluid on the shell's side in the tiny gaps within the baffles for the same overall cut ratio. This results in a bigger pressure drop for the shell side flow at the location of the baffles and permits a greater portion of the fluid to axially move in line with the tube bases. This produces reduced heat transmission as compared to the outcomes of integrating edge-cutting baffles, which permit the flow to go back and forth across the tube bundle along the entire length of the tubes between the baffles and deliver higher heat transfer rates.

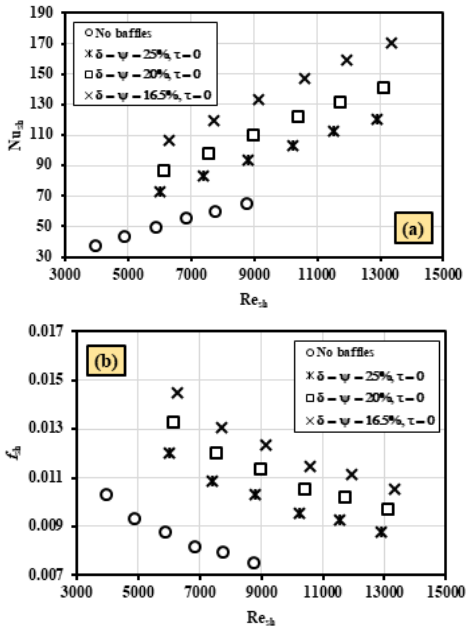

Fig. 9 Effect of baffle edge cut ratio without internal cutting on performance parameters (SCTs, β = 39.4%, τ = 0, λ = 1.97); (a) $\overline{Nu}_{sh}$, (b) f_{sh}.

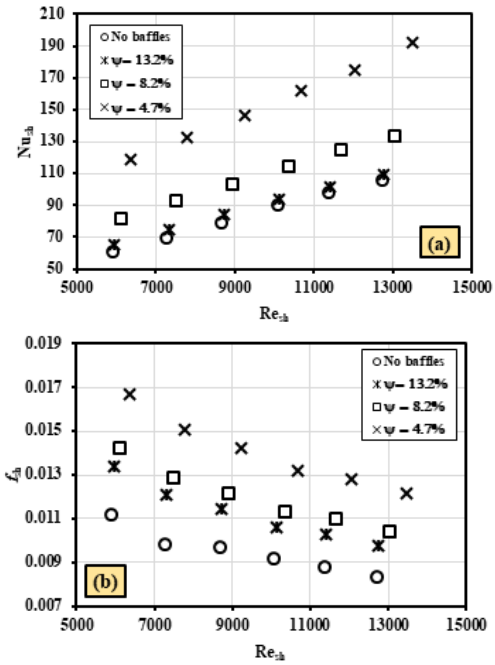

Fig. 10 Effect of baffle edge cut ratio with internal cutting on performance parameters (SCTs, β = 39.4%, τ = 11.8%, λ = 1.97); (a) $\overline{Nu}_{sh}$, (b) f_{sh}.

7.3 Heat exchanger with baffles at different pitch ratios

In this study, eight heat exchangers are subjected to 144 experimental tests; four of the heat exchangers have CCTs, while the other four have SCTs, with a base spacing of 7 mm (β = 55.1%). During the runs, edge-cut baffles are taken into consideration, with a ratio of δ = ψ =16.5% and τ = 0. The runs also consider three different pitch ratios: λ = 1.47, 1.97, and 2.36. The matching number of the included baffles is 5, 6, and 8, respectively, with 150 mm, 200 mm, and 250 mm as the baffles' respective pitches as revealed in Table 1. In these tests, pure cold water is fed through the shell of each heat exchanger in accordance with the standards listed in Table 2 while hot water with an intake temperature of 60°C and a total flow rate of 42.7 l/min circulates through the tubes. Fig. 11 displays the $\overline{\mathrm{Nu}}_{\mathrm{sh}}$ and f_{sh} recorded findings at β = 55.1%, $T_{sh,i}$ = 15°C, δ = ψ = 16.5%, τ = 0 as a sample of the results. It is seen that the inclusion of baffles in the heat exchanger raises both $\overline{\mathrm{Nu}}_{\mathrm{sh}}$ and f_{sh}. However, as the pitch ratio of the baffles increases, these performance metrics fall dramatically. When compared to no baffles, the average percentage improvements in the $\overline{\mathrm{Nu}}_{\mathrm{sh}}$ are 75.2%, 55.4%, and 46.7% at λ = 1.47, 1.97, and 2.36, respectively, for CCTs, and 88.1%, 67.8%, and 57.1% for SCTs. Furthermore, the typical percentage increases in the f_{sh} for CCTs are 29.9%, 19.2%, and 13.8% at λ = 1.47, 1.97, and 2.36, respectively, and 35.1%, 24.2%, and 18% for SCTs. By decreasing the pitch between the baffles, the likelihood of turbulence for the shell-side flow is increased, which in turn improves the impingement. This is because the increased number of baffles results in a significant enhancement of heat transfer. However, the trade-off for this improvement is a significant increase in pressure drop. In simpler terms, a closer distance between baffles causes more turbulence and better impingement, leading to better heat transfer, but at the expense of higher pressure drop.

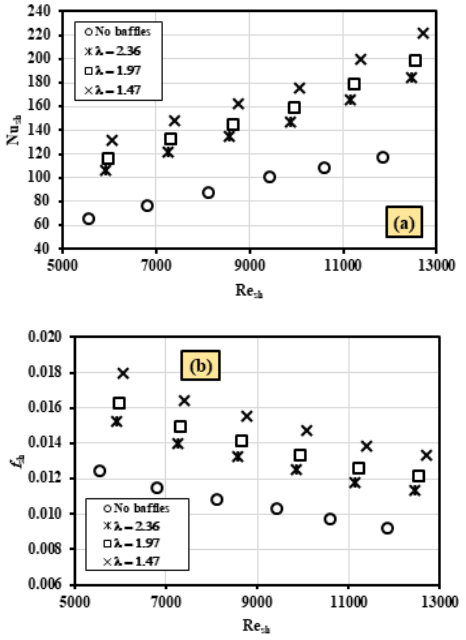

Fig. 11 Effect of baffle pitch ratio on performance parameters (β = 55.1%, $T_{sh,i}$ = 15°C, δ = ψ = 16.5%, τ = 0); (a) $\overline{Nu}_{sh}$, (b) f_{sh}.

7.4 Hydrothermal performance index

The SCTs and/or baffles should boost heat transmission more than the corresponding increase in fluid pumping force for a heat exchange approach to be regarded as a successful tool. This work assesses the hydrothermal performance index (HTPI) via St_{sh} and f_{sh} ratios [41,42] estimated using SCTs/baffles and CCTs as heat transfer surfaces, as presented in Eq. (28): in which $St_{sh,m}$ and $f_{\mathrm{sh,m}}$ reflect the modified Stanton number and Fanning friction factor, respectively, referring to the shell-side in heat exchangers with SCTs, and/or baffles. In addition, $St_{sh,0}$ and $f_{\mathrm{sh,0}}$ represent the corresponding Stanton number and Fanning friction factor of the shell-side at the same shell-side flow rate and inlet temperature, without baffles and equipped with CCTs. This equation is used to track the increase in heat transfer rate and shell-side flow resistance. This explanation aims to clarify the significance of the equation in relation to monitoring heat transfer and flow resistance in heat exchangers by engaging the proposed tested techniques.

$$HTPI = \frac{\mathrm{St_{sh,m}/St_{sh,0}}}{\left(f_{\mathrm{sh,m}}/f_{\mathrm{sh,0}}\right)^{1/3}} \quad (28)$$

Fig. 12a illustrates that raising the SCTs base spacing ratio increases the HTPI, and this increase is grown by installing baffles and reducing their cut ratio as indicated in Fig. 12b. In the absence of baffles, the average HTPI is 1.17 and 1.35 when CCTs are replaced with SCTs with base spacing ratios of 23.6% and 55.1%, respectively. Furthermore, when CCTs are replaced with SCTs with base spacing ratios of 23.6% and 55.1%, the average HTPI is 1.74 and 2.09, respectively, at a cut ratio of δ = ψ = 16.5%. The corresponding average HTPI values at δ = ψ = 25% are 1.31 and 1.54, respectively. In addition, Fig. 12c illustrates the average HTPI for different edge cut ratios (δ = ψ, τ = 0) of the baffles that are integrated with a pitch ratio of λ = 1.97. The results ensure that decreasing the baffle-edge cut ratio augments the HTPI. When CCTs and SCTs (β = 55.1%) are utilized, the average HTPI value at δ = ψ = 16.5% is 1.45 and 2.09, respectively. While at δ = ψ = 25%, the corresponding average HTPI falls to 1.09 and 1.54, respectively.

Fig. 12d also shows the average HTPI for several cutting configurations in the baffles (δ = 16.5%, λ = 1.97). It is demonstrated that given a fixed total cut ratio, increasing the internal cut ratio, and reducing the edge cut ratio results in a modest rise in the HTPI. However, it is evident that simply using the edge cutting is superior to using both internal and edge cuts. It is shown that the HTPI is 2.09 at δ = ψ = 16.5%, and 2.06 at δ = τ = 16.5%. Additionally, the average HTPI of the tested heat exchanger with engaged single segmental baffles at various pitch ratios (1.47 to 2.36) is shown in Fig. 12e. The findings are shown for δ = ψ = 16.5%, τ = 0. Raising the pitch between the baffles decreases the HTPI somewhat. The average HTPI value at λ = 1.47% when CCTs and SCTs (β = 55.1%) are used is 1.58 and 2.25, respectively. While λ = 2.36% reduces the corresponding average HTPI to 1.39 and 1.98, respectively.

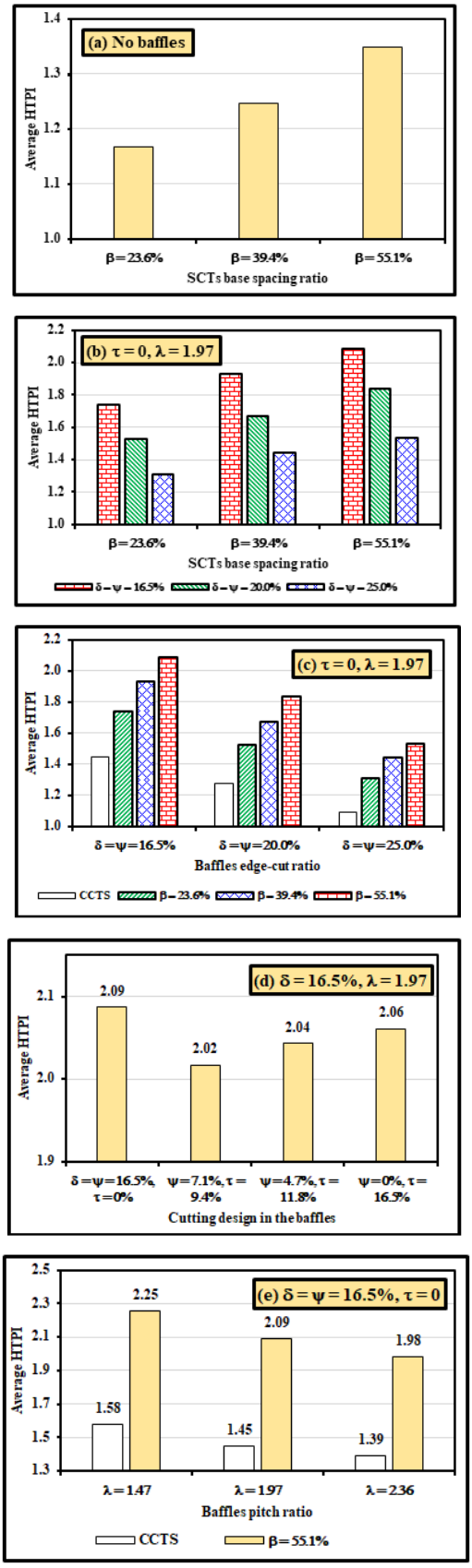

Fig. 12 The *HTPI* of the tested heat exchangers at different design settings.

8. Correlations

The average Nusselt number and Fanning friction factor of the shell side, besides the HTPI of the tested heat exchangers, are all predicted using the collected data in a sequence of correlations. For shell-tube heat exchangers without baffles, Eqs. (29-31) are applicable to cooling water flowing through the shell side of a counter-flow heat exchanger having CCTs or SCTs with base spacing ratios ranging from 23.6% to 55.1%. In addition, the Reynolds and Prandtl numbers on the shell side range from 3550 to 13900 and 4.78 to 7.28, respectively.

$$\overline{Nu}_{sh} = 0.0435\, Re_{sh}^{0.7081}\, Pr_{sh}^{0.4755}\, (1+\beta)^{0.8789} \quad (29)$$

$$f_{sh} = 0.2553\, Re_{sh}^{-0.3889}\, (1+\beta)^{0.7354} \quad (30)$$

$$HTPI = 0.6895\, Re_{sh}^{-0.0339}\, Pr_{sh}^{0.4043}\, (1+\beta)^{0.6717} \quad (31)$$

For heat exchangers with single segmental baffles, Eqs. (32-34) are applicable for cooling water passing through the shell side of a counter flow heat exchanger with CCTs or SCTs with base spacing ratios ranging from 23.6% to 55.1%. Besides, the baffle configuration has cut ratio specifications of $16.5\% \le \delta \le 25\%$, $0\% \le \psi \le 25\%$, and $0\% \le \tau \le 16.5\%$, and a pitch ratio range of $1.47 \le \lambda \le 2.36$. Furthermore, the shell-side Reynolds and Prandtl values range from 3585 to 14580 and 4.47 to 7.22, respectively.

$$\overline{Nu}_{sh} = 0.3707\, Re_{sh}^{0.661}\, Pr_{sh}^{0.3147}\, (1+\beta)^{1.02}\, (1+\psi)^{-5.0339}\, (1+\tau)^{-5.0237}\, \lambda^{-0.3608} \quad (32)$$

$$f_{sh} = 0.5694\, Re_{sh}^{-0.3838}\, (1+\beta)^{0.8593}\, (1+\psi)^{-2.6183}\, (1+\tau)^{-1.8597}\, \lambda^{-0.3427} \quad (33)$$

$$HTPI = 7.3506\, Re_{sh}^{-0.0919}\, Pr_{sh}^{-0.009}\, (1+\beta)^{0.8918}\, (1+\psi)^{-4.0619}\, (1+\tau)^{-3.838}\, \lambda^{-0.2737} \quad (34)$$

Comparing experimental $\overline{\mathrm{Nu}}_{\mathrm{sh}}$, f_{sh}, and HTPI values to those predicted by correlations is shown in Figs. 13 and 14. As shown, the proposed correlations agree with the most recent experimental results. For the exchangers without baffles (Eqs. (29-31)), it can be shown from Fig. 13 that all data are anticipated using the provided equations, with maximum variations of 3.5%, 4.6%, and 4.1% for $\overline{\mathrm{Nu}}_{\mathrm{sh}}$, f_{sh}, and HTPI, respectively. Fig. 14 demonstrates that the values for the exchangers with engaged single segmental baffles (Eqs. (32-34)) are predicted with maximum deviations of 8.2%, 7.2%, and 11.1% for $\overline{\mathrm{Nu}}_{\mathrm{sh}}$, f_{sh}, and HTPI, respectively.

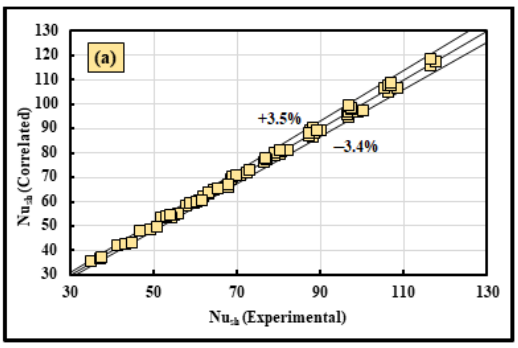

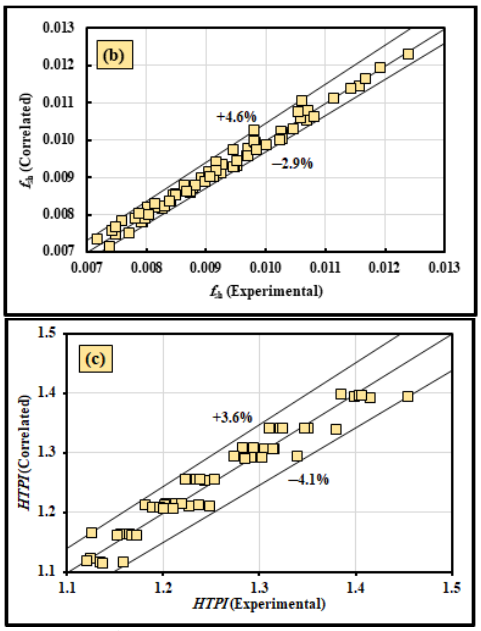

Fig. 13 Comparisons of the experimental values with that correlated by Eqs. (29-31); **(a)** $\overline{Nu}_{sh}$, **(b)** f_{sh}, **(c)** HTPI.

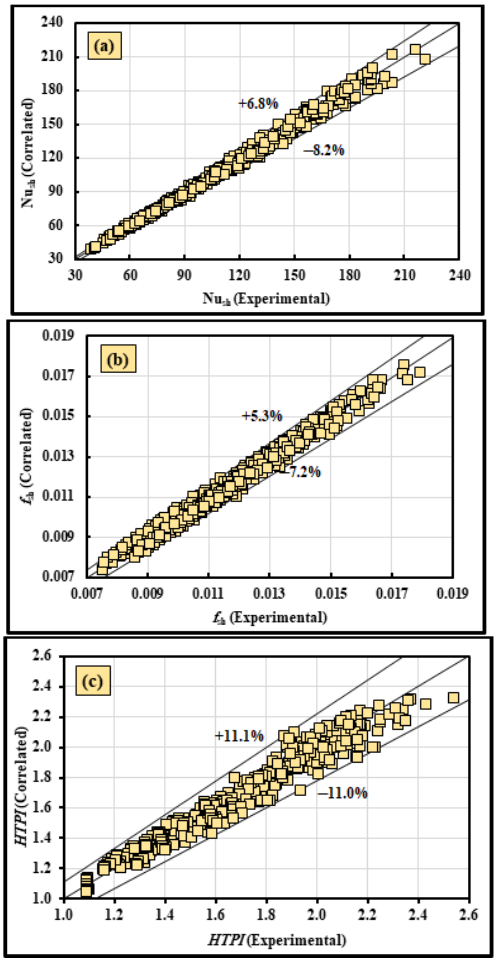

Fig. 14 Comparisons of the experimental values with that correlated by Eqs. (32-34); **(a)** $\overline{Nu}_{sh}$, **(b)** f_{sh}, **(c)** HTPI.

9. Conclusions

This study presents an experimental investigation of the hydrothermal attributes of a shell-tube heat exchanger of a counter flow configuration which, includes CCTs or SCTs of different base spacing ratios ($23.6\% \le \beta \le 55.1\%$). In addition, single segmental baffles with different cut configurations and ratios ($16.5\% \le \delta \le 25\%$, $0\% \le \psi \le 25\%$, $0\% \le \tau \le 16.5\%$) and pitch ratios ($1.47 \le \lambda \le 2.36$) are considered. A total of 522 tests were carried out on 29 heat exchangers for a variety of Reynolds numbers ($3550 \le Re_{sh} \le 14580$) and Prandtl numbers ($4.47 \le Pr_{sh} \le 7.28$). The results may be summarized as follows:

- When SCTs are used instead of CCTs, the heat transfer coefficient and friction factor are increased. Furthermore, these performance parameters are further increased with expanding the SCT spacing ratio.
- The baffles' mere existence in the heat exchanger raises both $\overline{Nu}_{sh}$ and f_{sh}, and by reducing the baffle edge cut ratio, these performance metrics considerably rise.
- The baffles with both edge and internal cuttings still achieve higher shell-Nusselt number and friction factor when compared with no baffle case. But baffles with edge cutting are a better tool than those with internal cutting.
- As the pitch ratio of the baffles increases, both $\overline{Nu}_{sh}$ and f_{sh} fall dramatically.
- The $\overline{Nu}_{sh}$ is reduced as the inlet temperature of the shell-fluid flow rises, while $T_{sh,i}$ have a negligibly little impact on f_{sh}.
- Raising Re_{sh} augments $\overline{Nu}_{sh}$, while f_{sh} is decreased.
- The HTPI is clearly more than one for all operating settings and increases with increasing SCTs base spacing ratio, and with decreasing the baffle cut ratio, baffle pitch ratio, shell-side flow rate, and/or intake temperature.
- The maximum HTPI is 2.54, achieved by utilizing baffles of $\delta = \psi = 16.5\%$, $\tau = 0$, $\lambda = 1.47$, and SCTs of $\beta = 55.1\%$, and lowest shell-side flow rate and inlet temperature.
- Correlations are introduced to predict the $\overline{Nu}_{sh}$ and f_{sh} as well as the HTPI of the tested heat exchangers.

References

[1] J. Wajs, M. Bajor, M. Bajor and D. Mikielewicz, "Thermal-Hydraulic Studies on the Shell-and-Tube Heat Exchanger with Minijets", Energies, vol. 12(17), Article ID 3276, 2019.

[2] B. Wang, J.J. Klemeš, N. Li, M. Zeng, P.S. Varbanov, Y. Liang, "Heat Exchanger Network Retrofit with Heat Exchanger and Material Type Selection: A review and a Novel Method", Renewable and Sustainable Energy Reviews, vol. 138, Article ID 110479, 2021.

[3] F.C. Euan Somerscales and Arthur E. Bergles "Enhancement of Heat Transfer and Fouling Mitigation", Advances in Heat Transfer, vol. 30, pp. 197–253, 1997.

[4] M.R. Salem, R.K. Ali, R.Y. Sakr and K.M. Elshazly, "Experimental Study on Convective Heat Transfer and Pressure Drop of Water-Based Nanofluid Inside Shell and Coil Heat Exchanger", PhD thesis, Faculty of Engineering at Shoubra, Benha University, 2014.

[5] M.R. Salem, M.K. Althafeeri, K.M. Elshazly, M.G. Higazy, M.F. Abdrabbo, "Experimental Investigation on the Thermal Performance of a Double Pipe Heat Exchanger with Segmental Perforated

Baffles", International Journal of Thermal Sciences, vol. 122, pp. 39-52, 2017.

[6] S.M. Elshamy, M.T. Abdelghany, M.R. Salem, O.E. Abdellatif, "Energy and Exergy Analysis of Shell and Coil Heat Exchanger using Water Based Al2O3 Nanofluid Including Diverse Coil Geometries: An Experimental Study", Journal of Nanofluids, vol. 9(1), pp. 13–23, 2020

[7] M.S. Avval and E. Damangir, "A General Correlation for Determining Optimum Baffle Spacing for All Types of Shell and Tube Exchangers", International Journal of Heat and Mass Transfer, vol. 38(13), pp. 2501-2506, 1995.

[8] G. Wang, K. Stone, and S.P. Vanka, "Unsteady Heat Transfer in Baffled Channel", ASME Journal of Heat Transfer, vol. 118, pp. 585-591, 1996.

[9] Z.D. Chen and J.J. Chen, "Local Heat Transfer for Oscillatory Flow in The Presence of a Single Baffle within a Channel", Chemical Engineering Science, vol. 53, pp. 3177-3180, 1998.

[10] M. Yilmaz, "The Effect of Inlet Flow Baffles on Heat Transfer", International Communications in Heat and Mass Transfer, vol. 30(8), pp. 1169-1178, 2003.

[11] Y. Yang and C. Hwang, "Calculation of Turbulent Flow and Heat Transfer in a Porous-Baffled Channel", International Journal of Heat and Mass Transfer, vol. 46, pp. 771-780, 2003.

[12] P. Dutta and A. Hossain, "Internal Cooling Augmentation in Rectangular Channel Using Two Inclined Baffles", International Journal of Heat and Fluid Flow, vol. 26, pp. 223-232, 2005.

[13] A. Tandiroglu and T. Ayhan, "Energy Dissipation Analysis of Transient Heat Transfer for Turbulent Flow in a Circular Tube with Baffle Inserts", Applied Thermal Engineering, vol. 26, pp. 178-185, 2006.

[14] S. Wang, J. Wen, and Y. Li, "An Experimental Investigation of Heat Transfer Enhancement for a Shell-And-Tube Heat Exchanger", Applied Thermal Engineering, vol. 29, pp. 2433–2438, 2009.

[15] H. Benzenine, R. Saim, S. Abboudi and O. Imine, "Numerical Simulation of the Dynamic Turbulent Flow Field through A Channel Provided with Baffles: Comparative Study between Two Models of Baffles: Transverse Plane and Trapezoidal", Revue des Energies Renouvelables, vol. 13(4), pp. 639–651, 2010.

[16] S. Eiamsa-ard and P. Promvonge, "Laminar Periodic Flow and Heat Transfer in a Rectangular Channel with Triangular Wavy Baffles", Journal of Thermal Science, vol. 21(3), pp. 250−261, 2012.

[17] H. Benzenine, R. Saim, S. Abboudi, and O. Imine, "Numerical Study on Turbulent Flow Forced-Convection Heat Transfer for Air in a Channel with Waved Fins", Mechanika. vol. 19(2), pp. 150-158, 2013.

[18] J. Zhang, S. Guo, Z. Li, J. Wang, Y. He, W. Tao, "Experimental Performance Comparison of shell-and-Tube Oil Coolers with Overlapped Helical Baffles and Segmental Baffles", Applied Thermal Engineering, vol. 58, pp. 336-343, 2013.

[19] K. Arslan and N. Onur, "Experimental Investigation of Flow and Heat Transfer in Rectangular Cross-Sectioned Duct with Baffles Mounted on the Bottom Surface with Different Inclination Angles", Heat Mass Transfer, vol. 50, pp. 169–181, 2014.

[20] S.A. Hussein, "Experimental Investigation of Double Pipe Heat Exchanger by using Semi Circular Disc Baffles", International Journal of Computer Applications, vol. 115(4), pp. 13-17, April 2015.

[21] A. Boonloi and W. Jedsadaratanachai, "Numerical Investigation on Turbulent Forced Convection and Heat Transfer Characteristic in A Square Channel with Discrete Combined V-Baffle and V-Orifice", Case Studies in Thermal Engineering, vol. 8, pp. 226-235, 2016.

[22] P.S.P. Amirtharaj, S. Allaudinbasha, M. Janagan, R. Karthikeyan, S. Muthukumar, "Design and Analysis of Shell and Tube Heat Exchanger with Inclined Baffles", International Journal of Scientific Development and Research, vol. 1(3), pp. 252-260, 2016.

[23] A.H. Falih, "Effect of Baffles Orientation on Heat Transfer Enhancement in Dimpled Square Duct", Journal of Engineering and Sustainable Development, vol. 21(3), pp. 36-46, 2017.

[24] A.B. Colaço, F. Bernardo, M.B. Lopes, V.C. Mariani, L.S. Coelho, M.R. Salem, "Optimization of Double Pipe-Heat Exchanger with Single Segmental Perforated Baffles", 17th Brazilian Congress of Thermal Sciences and Engineering November 25th-28th, 2018, Águas de Lindóia, SP, Brazil.

[25] M.R. Salem, M. Eltoukhey, R. Ali, K. Elshazly, "Experimental Investigation on the Hydrothermal Performance of a Double-Pipe Heat Exchanger using Helical Tape Insert", International Journal of Thermal Sciences, vol. 124, pp. 496-507, 2018.

[26] P. Bichkar, O. Dandgaval, P. Dalvi, R. Godase, T. Dey, "Study of Shell and Tube Heat Exchanger with the Effect of Types of Baffles", Procedia Manufacturing, vol. 20, pp. 195-200, 2018.

[27] M.H. Mohammadi, H.R. Abbasi, A. Yavarinasab, H. Pourrahmani, "Thermal Optimization of Shell and Tube Heat Exchanger using Porous Baffles", Applied Thermal Engineering, vol. 170, Article ID 115005, 2020.

[28] A. Youcef and R. Saim, "Numerical Analysis of the Baffles Inclination on Fluid Behavior in a Shell and Tube Heat Exchanger", Journal of Applied Computational Mechanics, vol. 7(1), pp. 312-320, 2021.

[29] S. Gaikwad and A. Parmar, "Numerical Simulation of the Effect of Baffle Cut and Baffle Spacing on Shell Side Heat Exchanger Performance using CFD", Chemical Product and Process Modeling, vol. 16(2), pp. 145-154, 2021.

[30] A.B. Colaço, V.C. Mariani, M.R. Salem, L.S. Coelho, "Maximizing the Thermal Performance Index Applying Evolutionary Multi-Objective Optimization Approaches for Double Pipe Heat Exchanger", Applied Thermal Engineering, vol. 211, Article ID 118504, 2022.

[31] A. Boonloi and W. Jedsadaratanachai, "Effects of Baffle Height and Baffle Location on Heat Transfer and Flow Profiles in a Baffled Duct: A CFD Analysis", Modelling and Simulation in Engineering, vol. 2022, Article ID 3698887, 19 pages, 2022.

[32] S. Akcay and U. Akdag, "Heat Transfer Enhancement in a Channel with Inclined Baffles Under Pulsating Flow: A CFD Study", Journal of Enhanced Heat Transfer, vol. 30(5), pp. 61-79, 2023.

[33] M.R. Salem, Experimental investigation on the hydrothermal attributes of MWCNT/water nanofluid in the shell-side of shell and semi-circular tubes heat exchanger", Applied Thermal Engineering, vol. 176, Article No. 115438, 2020.

[34] M. Moawed, "Thermal Performance of a Cross Flow Heat Exchanger with Semi-Circular Tubes", ERJ Shoubra Faculty of Engineering, vol. 4, pp. 87-109, June 2005.

[35] S.A. Nada, H. El-Batsh, M. Moawed, "Heat Transfer and Fluid Flow Around Semi-Circular Tube in Cross Flow at Different Orientations", Heat Mass Transfer, vol. 43, pp. 1157-1169, 2007.

[36] E.Z. Ibrahiem, A.O. Elsayed, "Heat Transfer Performance of a Semi-Circular Tube Bank", Heat Transfer Research, vol. 46(6), pp. 563-576, 2015.

[37] F.W. Dittus and L.M.K. Boelter, "Heat Transfer in Automobile Radiators of the Tubular Type", University of California Publications in Engineering, 1930, 2,443461. Lawrence, A. E.

[38] S.J. Kline and F.A. McClintock, "Describing Uncertainties in Single-Sample Experiments", Mechanical Engineering, vol. 75(1), pp. 3–8, January 1953.

[39] V. Gnielinski, "New Equations for Heat and Mass Transfer in Turbulent Pipe and Channel Flow", International Chemical Engineering, vol. 16, pp. 359–368, 1976.

[40] G.K. Filonenko, "Hydraulic Resistance of Pipes (Hydraulischer Widerstand von Rohrleitungen)," Teploenergetika, vol. 1(4), pp. 40-44, 1954.

[41] M.R. Salem, M. Eltoukhey, R. Ali, K. Elshazly, "Experimental Investigation on the Hydrothermal Performance of a Double-Pipe Heat Exchanger using Helical Tape Insert", International Journal of Thermal Sciences, vol. 124, pp. 496-507, 2018.

[42] H.H. Al-Kayiem, A. Bin Ekhwan, L.N. Muhi, "Augmentation of Ribs Turbulators Height on the Hydrothermal Performance of Double Pipe Heat Exchanger", Journal of Engineering Science and Technology, vol. 12(2), pp. 548-563, 2017.

Nomenclatures

A	Area, m^2
Cp	Specific heat at constant pressure, $J/kg.℃$
d	Diameter, m
f	Fanning friction factor
h	Convection heat transfer coefficient, $W/m^2.℃$
k	Thermal conductivity, $W/m.℃$
L	Length, m
m	Mass, kg
$\dot{m}$	Mass flow rate, kg/s
N	Number
P	Pressure, Pa
p	Pitch, m
Q	Heat transfer rate, W
S	Spacing, m
T	Temperature, ℃
U	Overall heat transfer coefficient, $W/m^2.℃$
u	Velocity, m/s
V	Volume, m^3
$\dot{V}$	Volume flow rate, m^3/s

Dimensionless groups

$\overline{Nu}$	Average Nusselt number
Pr	Prandtl number
Re	Reynolds number
St	Stanton number

Greek letters

β	Base spacing ratio
δ	Baffles cut ratio
Δ	Differential
ψ	Edge cut ratio
λ	Baffles pitch ratios
ω	Uncertainty
μ	Dynamic viscosity, $kg/m.s$
π	Pi ≡ A mathematical constant ≅ 3.1416
ρ	Density, kg/m^3
τ	Internal cut ratio

Superscripts and subscripts

0	No modification
ave	Average
b	Base
h	Hydraulic
i	Inner or inlet or internal
LM	Logarithmic Mean
m	Modified
o	Out or outer
sh	Shell
t	Tube

Acronyms and abbreviations

CCT	Complete Circular Tube
HTPI	Hydrothermal Performance Index
SCT	Semi-Circular Tube